Supporting Information

Ce-doped IrO_2 Electrocatalysts with Enhanced Performance for Water Oxidation in Acidic Media

YaHui Wang,[†#] *Shaoyun Hao,*[†#] *Xiangnan Liu,*[†] *Qiqi Wang,*[†] *Zhiwei Su,*[†] *Lecheng Lei,*[†,‡] *Xingwang Zhang**[,†,‡]

[†]Key Laboratory of Biomass Chemical Engineering of Ministry of Education, College of Chemical and Biological Engineering, Zhejiang University, Zheda Road 38, Hangzhou, Zhejiang Province 310027, China

[‡]Institute of Zhejiang University-Quzhou, 78 Jiuhua Boulevard North, Quzhou, Zhejiang Province 324000, China

E-mail: xwzhang@zju.edu.cn

Calculations for electrochemical measurements and theoretical calculation detials

Calculation of ECSA

In addition, the ECSA of catalyst on GCE is calculated according to the equation:

$$ECSA = C_{dl}/C_s \qquad \text{Equation (1)}$$

Where the C_s is the specific capacitance value in 0.5 M H_2SO_4.

Calculation of Faradaic efficiency

The oxygen generated at working anode in 0.5 M H_2SO_4 solution was confirmed by gas chromatography analysis (GC, 9790II, Hangzhou Gatai Scientific Instruments) and quantitatively measured by using an electrolytic cell. The FE was calculated by comparing the amount of experimentally measured oxygen generated by potentiostatic anodic electrolysis with theoretically calculated oxygen.

The Faradaic efficiency (FE) was calculated according to the following equation:

$$\text{FE } (O_2, \%) = \frac{V_{O_2} \cdot 4 \cdot F}{V_m \cdot i \cdot t} \cdot 100\% \qquad \text{Equation (2)}$$

Where V_{O2} represents the volume of generated O_2, F is the Faraday constant (96485.33289 C/mol), V_m is the molar volume of the gas, i is the current, and t is the time for electrolysis.

Calculation of TOF

To estimate the concentration of active site, the TOF values were calculated by the following equation:

$$\text{TOF} = \frac{j \cdot A}{4F \cdot n} \qquad \text{Equation (3)}$$

Where j is the current density (mA cm^{-2}) at defined overpotential. A represents the surface area of testing electrode (cm^2). 4 means mole of electrons consumed for evolving one mole O_2 from water. F is the Faradic constant (96,485.3 C mol^{-1}), and n is the moles of Ir atoms on the

prepared working electrode which could be calculated from the loading weight of electrocatalysts on CP.

Theoretical calculation

The present first principle DFT calculations are performed by Vienna Ab initio Simulation Package (VASP)[1] with the projector augmented wave (PAW) method.[2] The exchange-functional is treated using the generalized gradient approximation (GGA) of Perdew-Burke-Ernzerhof (PBE)[3] functional. The cut-off energy of the plane-wave basis is set at 500 eV for optimize calculations of atoms and cell optimization. The vacuum spacing in a direction perpendicular to the plane of the catalyst is at least 20 Å. The Brillouin zone integration is performed using 3×3×1 Monkhorst and Pack[4] k-point sampling for a primitive cell. A 5×5×1 Monkhorst and Pack k-point sampling was used in calculating the density of state (DOS). The self-consistent calculations apply a convergence energy threshold of 10^{-4} eV. The maximum Hellmann-Feynman force for each ionic optimization step is 0.025eV/Å. The equilibrium lattice constants were optimized with maximum stress on each atom within 0.01 eV/Å. Spin polarizations was considered in all calculations.

There are six types of doping in the IrO_2, including IrO_2 (initial); $Ce_{0.2}$-IrO_2-1; $Ce_{0.2}$-IrO_2-2; $Ce_{0.2}$-IrO_2-3; $Ce_{0.2}$-IrO_2-4; $Ce_{0.2}$-IrO_2-5; $Ce_{0.2}$-IrO_2-6.

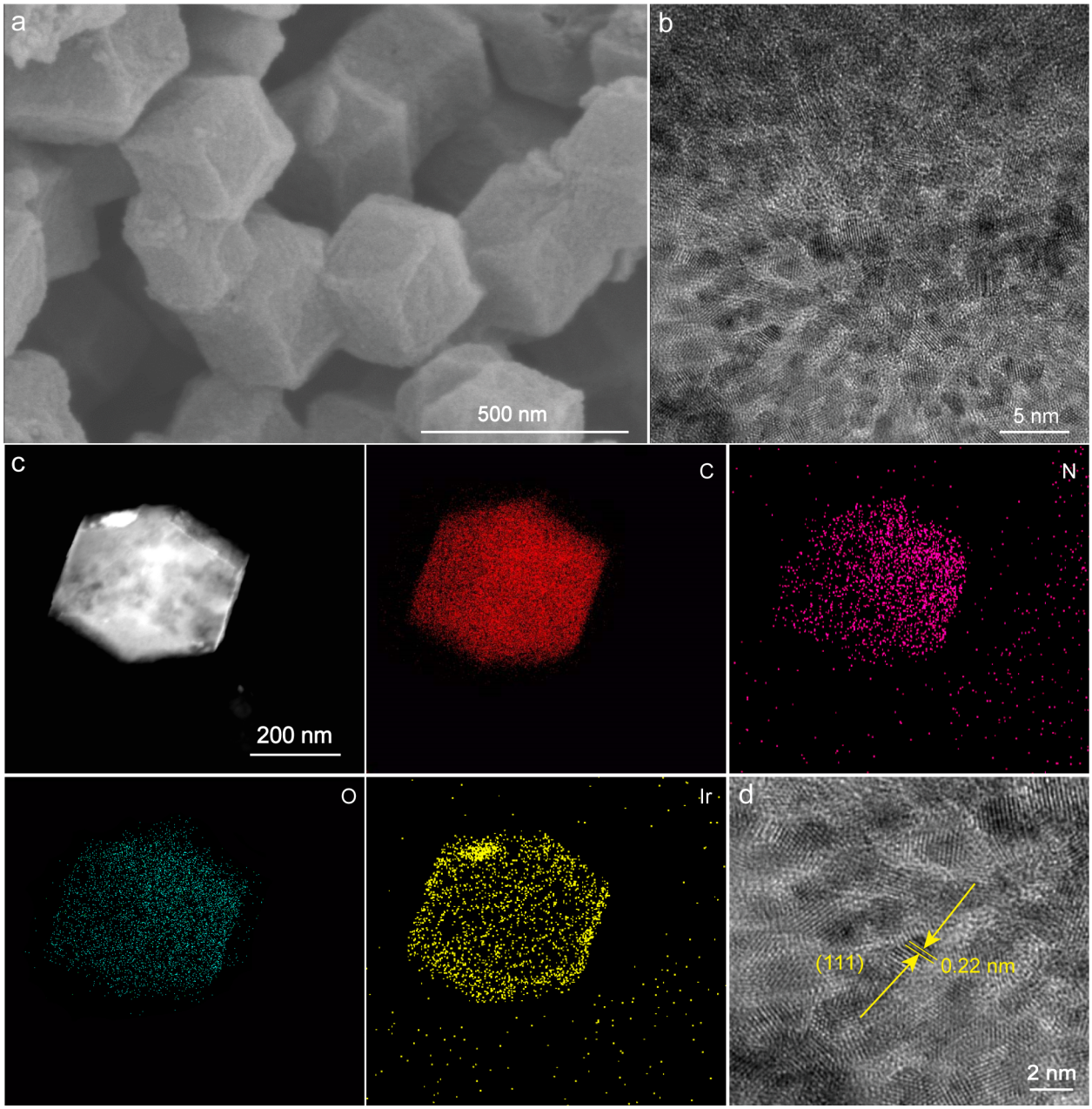

Figure S1. (a) SEM image, (b) HR-TEM image, (c) TEM image and elemental maps, (d) high-magnification HR-TEM image for IrO_2@NPC.

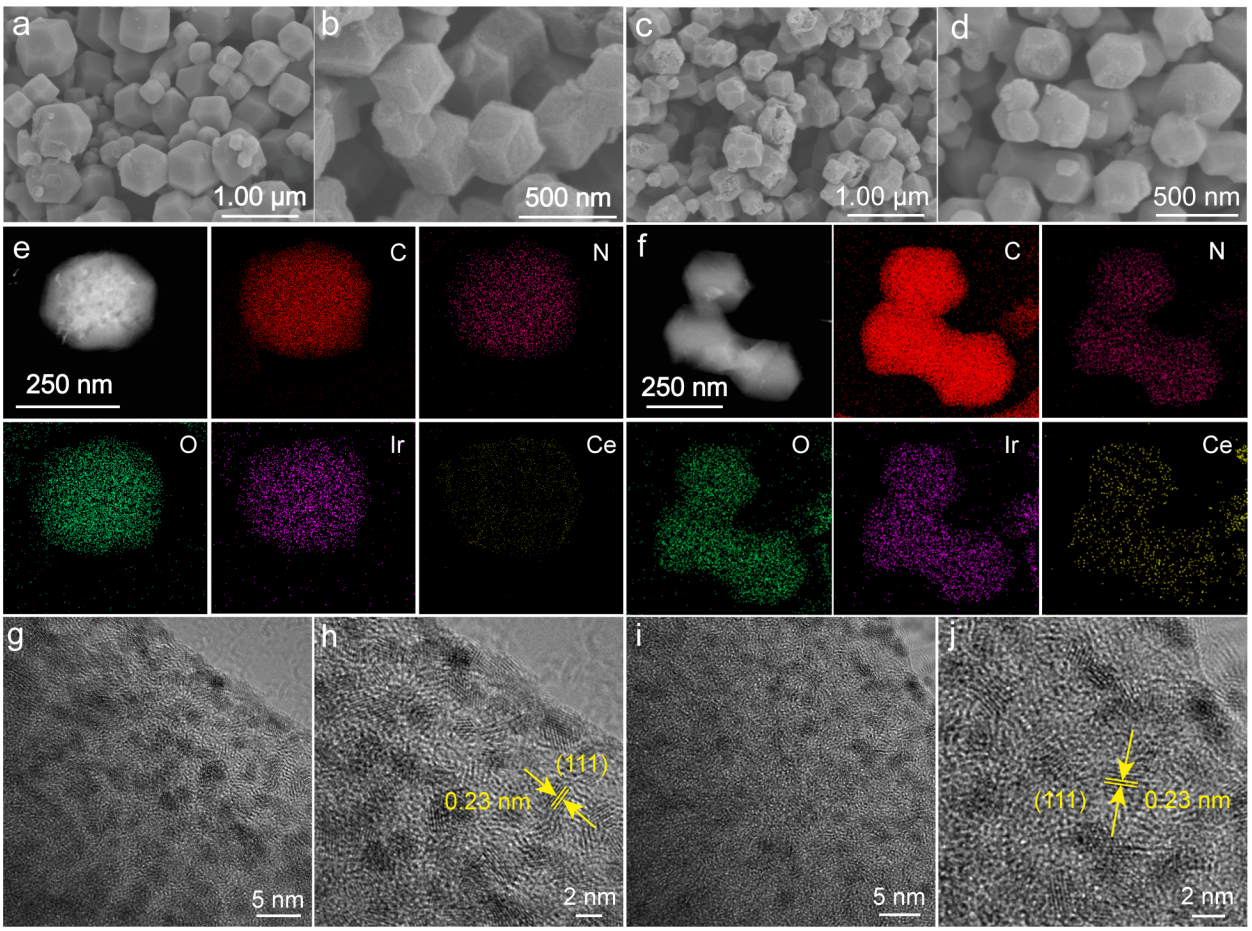

Figure S2. (a) SEM image, (b) high-magnification SEM image for $Ce_{0.15}$-IrO_2@NPC. (c) SEM image, (d) high-magnification SEM image for $Ce_{0.25}$-IrO_2@NPC. TEM image and elemental maps for (e) $Ce_{0.15}$-IrO_2@NPC, (f) $Ce_{0.25}$-IrO_2@NPC. (g) HR-TEM image, (h) high-magnification HR-TEM image for $Ce_{0.15}$-IrO_2@NPC. (i) HR-TEM image, (j) high-magnification HR-TEM image for $Ce_{0.25}$-IrO_2@NPC.

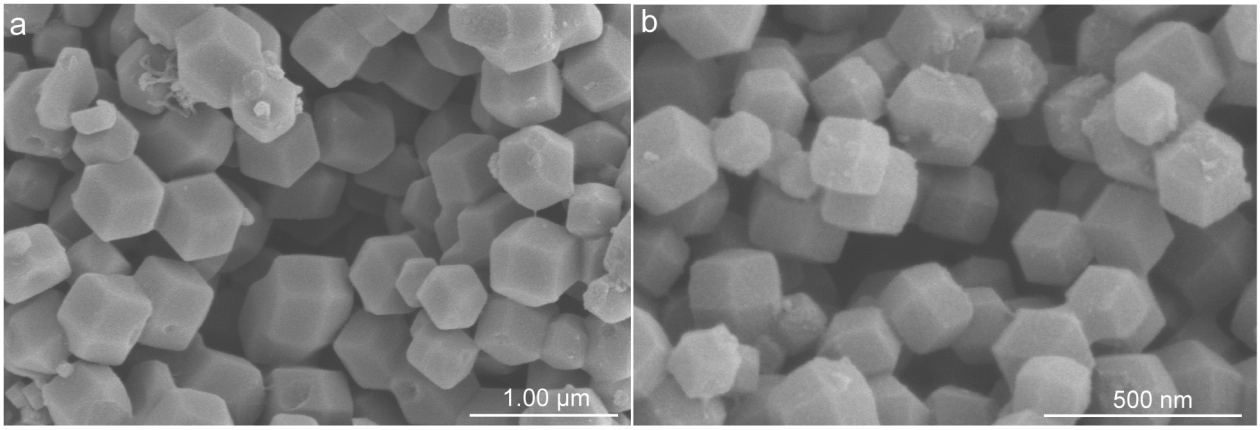

Figure S3. SEM images for $Ce_{0.2}$-IrO_2@NPC.

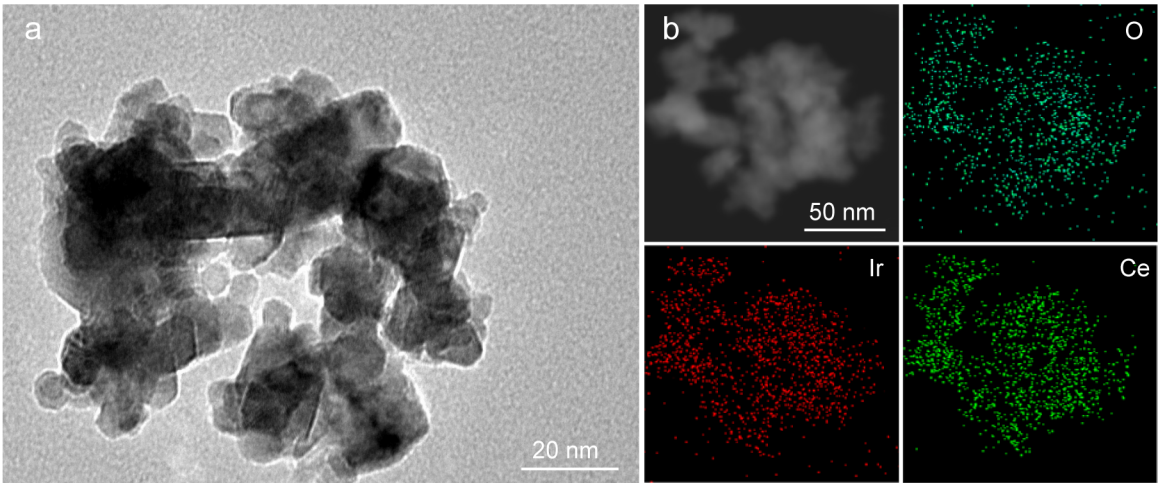

Figure S4. TEM image and elemental maps for $Ce_{0.2}$-IrO_2 without substrate.

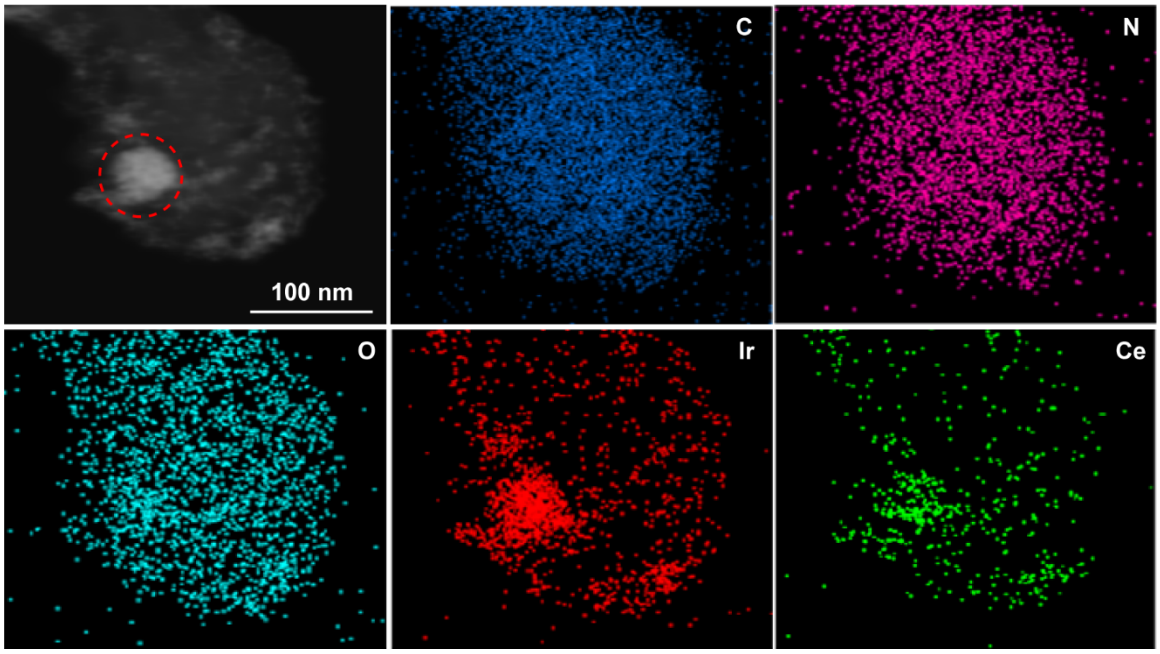

Figure S5. TEM image and elemental maps for $Ce_{0.2}$-IrO_2@NPC (15 wt%).

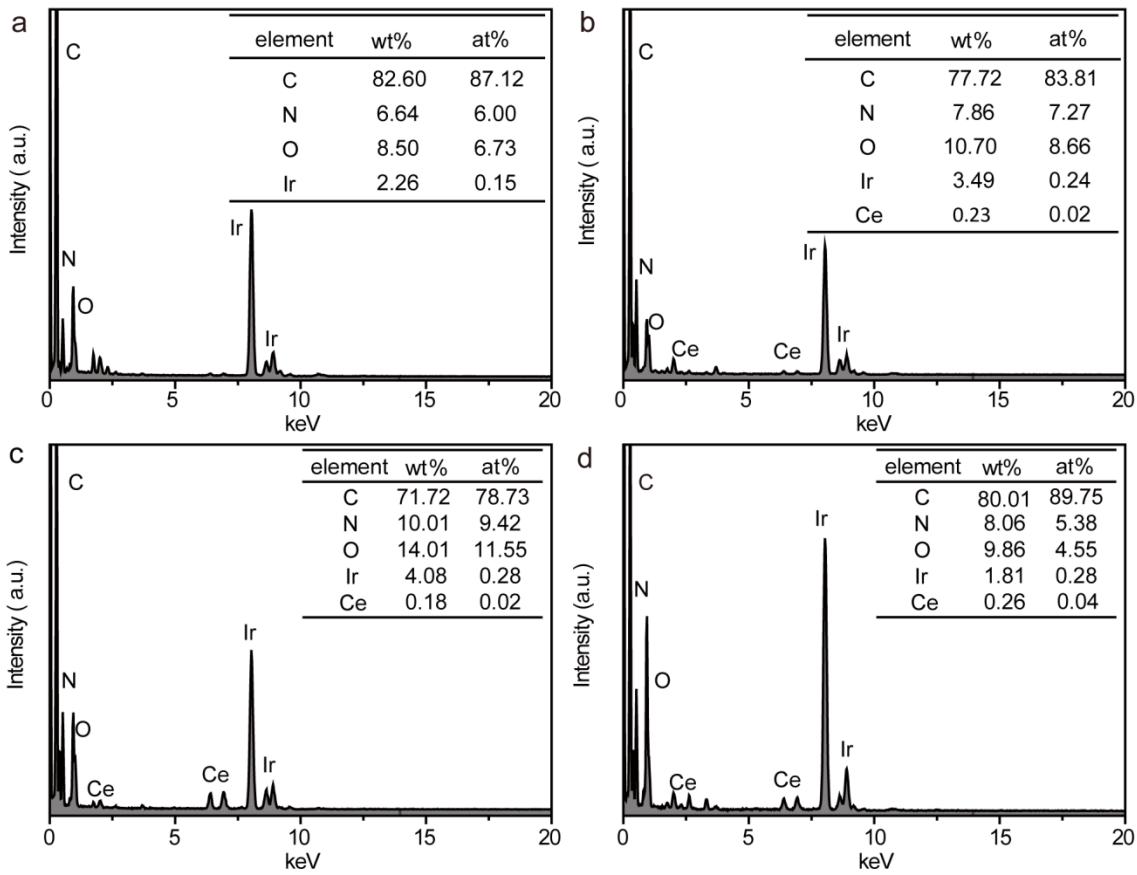

Figure S6. EDX analysis for (a) IrO_2@NPC, (b) $Ce_{0.15}$-IrO_2@NPC, (c) $Ce_{0.2}$-IrO_2@NPC, (d) $Ce_{0.25}$-IrO_2@NPC.

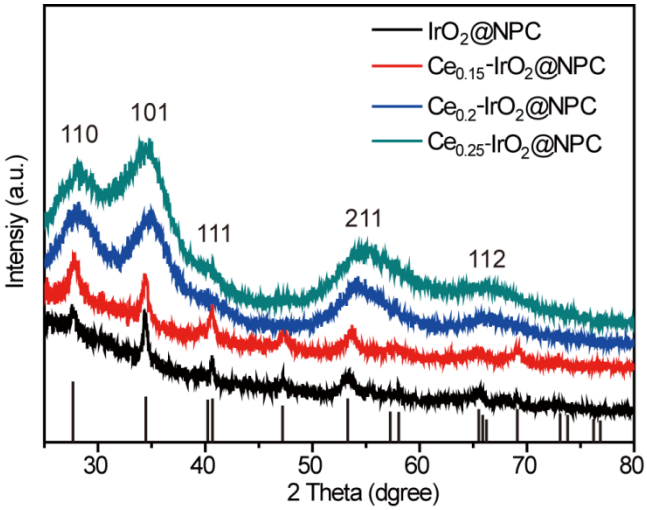

Figure S7. XRD patterns for IrO_2@NPC, $Ce_{0.15}$-IrO_2@NPC, $Ce_{0.2}$-IrO_2@NPC, $Ce_{0.25}$-IrO_2@NPC (PDF: #15-0870).

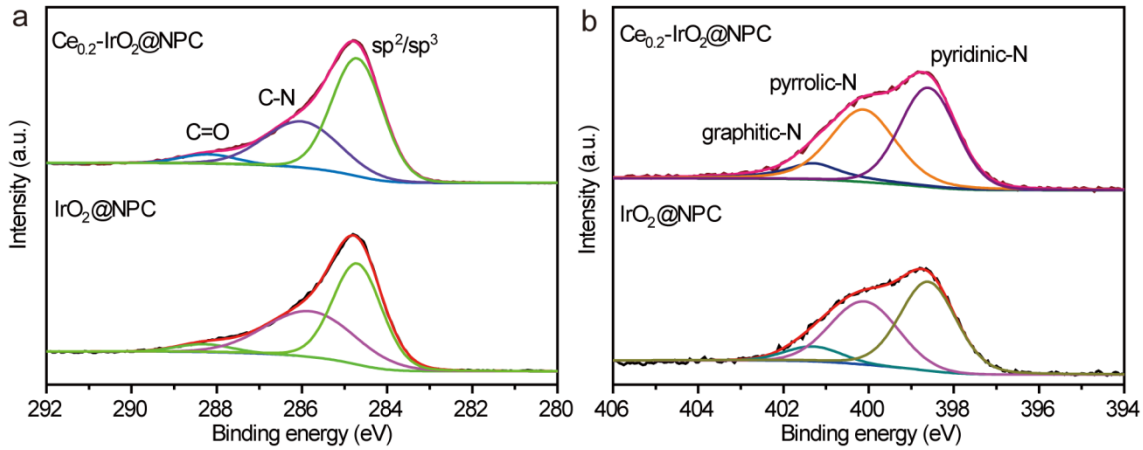

Figure S8. The high-resolution XPS for (a) C 1s, (b) N 1s.

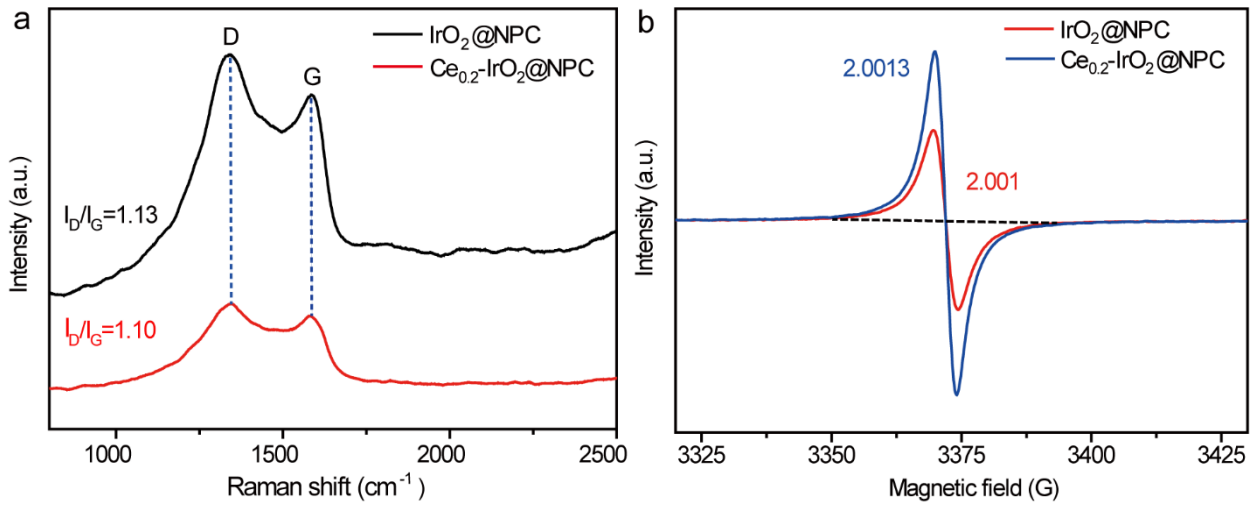

Figure S9. (a) Raman spectra for IrO_2@NPC and $Ce_{0.2}$-IrO_2@NPC, (b**)** ESR spectra for IrO_2@NPC and $Ce_{0.2}$-IrO_2@NPC.

Table S1. Comparison of some representative Ir-based OER catalysts reported under acidic conditions.

Catalysts	Electrolyte solution	Stability	Overpotentials (vs RHE) at j=10mA cm^{-2}	Reference
Ir-STO	0.1 M $HClO_4$	20 h	247 mV	*Angew. Chem. Int. Ed.* **2019**, 58, 7631
$IrO_x/SrIrO_3$	0.5 M H_2SO_4	30 h	~270 mV	*Science* **2016**, 353, 1011
Sr_2CoIrO_6	0.1 M $HClO_4$	24 h	330 mV	*Angew. Chem. Int. Ed.* **2019**, 58, 4571
IrO_2/CNT	0.5 M H_2SO_4	10 h	293 mV	*ACS Catal.* **2017**, 7, 5983
Ru@IrO_x	0.05 M H_2SO_4	24 h	282 mV	*Chem.* **2019**, 5, 1
Ir_6Ag_9NTs/C	0.5 M H_2SO_4	6 h	285 mV	*Nano Energy* **2019**, 56, 330
Co-RuIr	0.1M $HClO_4$	25 h	235 mV	*Adv. Mater.* **2019**, 31, 1900510
$Ir_{0.5}(NiCo_{1.5})_{0.5}O_\delta$	0.1 M $HClO_4$	5.56 h	285 mV	*ACS Energy Lett.* **2017**, 2, 2786
P-$IrCu_{1.4}$NCs	0.05 M H_2SO_4	10 h	311 mV	*Chem. Mater.* **2018**, 30, 8571
np-IrO_2	0.5 M H_2SO_4	40 h	240 mV	*ACS Appl. Energy Mater.* **2020**, 3, 4, 3736
Ir-SA@Fe@NCNT	0.5 M H_2SO_4	12 h	250 mV	*Nano Lett.* **2020**, 20, 3, 2120
$Ce_{0.2}$-IrO_2@NPC	**0.5 M H_2SO_4**	**100 h**	**224 mV**	**This work**

Table S2. ICP analysis for $Ce_{0.2}$-IrO_2@NPC after stability test

Element	After 5 h	After 20 h	After 50 h	After 100 h
Ir	2.6 ppb	5.4 ppb	14.1 ppb	27.3 ppb
Ce	0.5 ppb	1.1 ppb	3.1 ppb	5.6 ppb

Table S3. Onset potential for the prepared catalysts

Catalysts	Onset potential (where EIS spectra are measured)
Commercial IrO_2	1.50 V
IrO_2@NPC	1.47 V
$Ce_{0.15}$-IrO_2@NPC	1.43 V
$Ce_{0.2}$-IrO_2@NPC	1.40 V
$Ce_{0.25}$-IrO_2@NPC	1.42 V

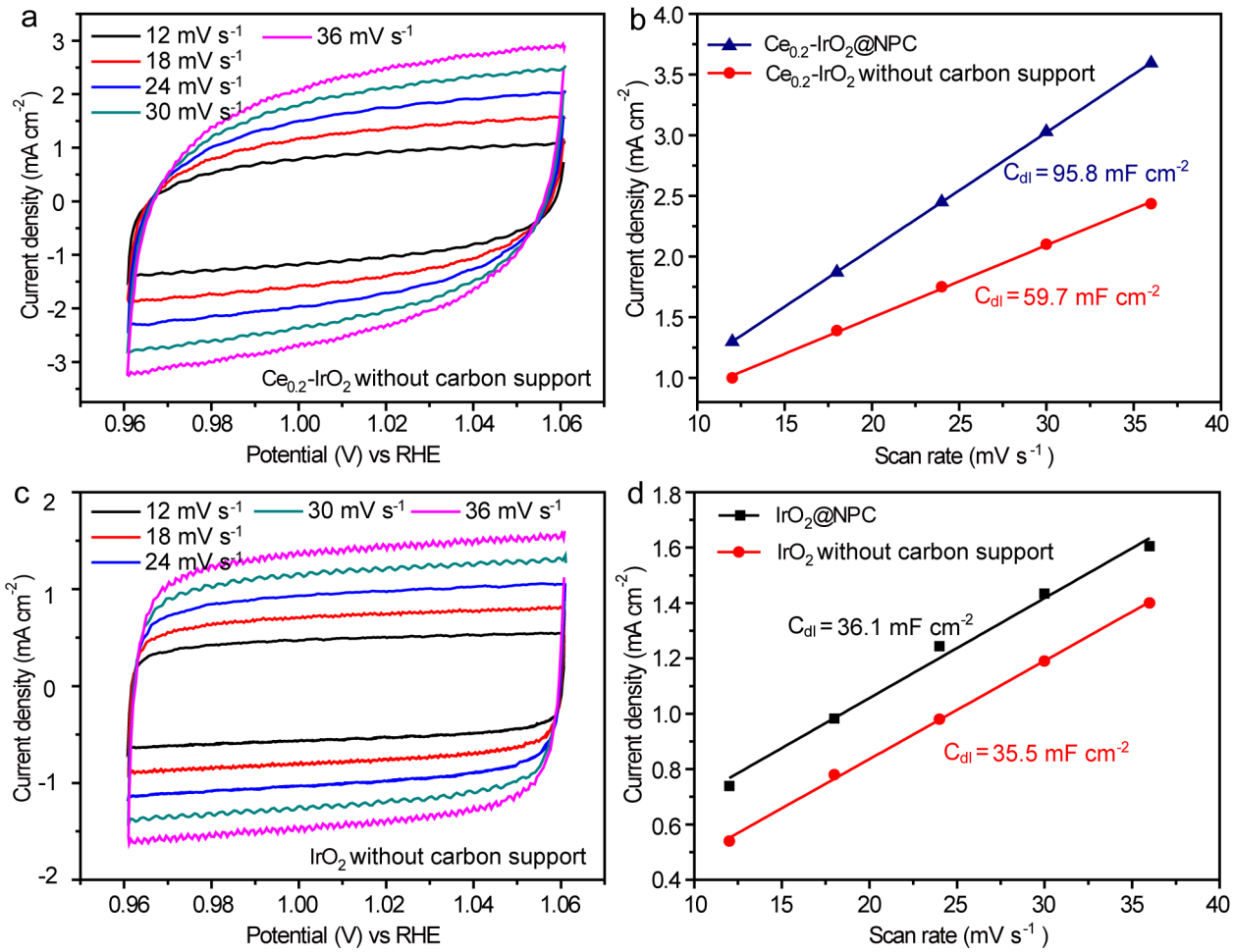

Figure S10. (a) CV curves and (b) C_{dl} estimated from the as-measured CV curves for $Ce_{0.2}$-IrO_2 without carbon support from 12 mV s^{-1} to 36 mV s^{-1}, (c) CV curves and (d) C_{dl} estimated from the as-measured CV curves for IrO_2 without carbon support from 12 mV s^{-1} to 36 mV s^{-1}.

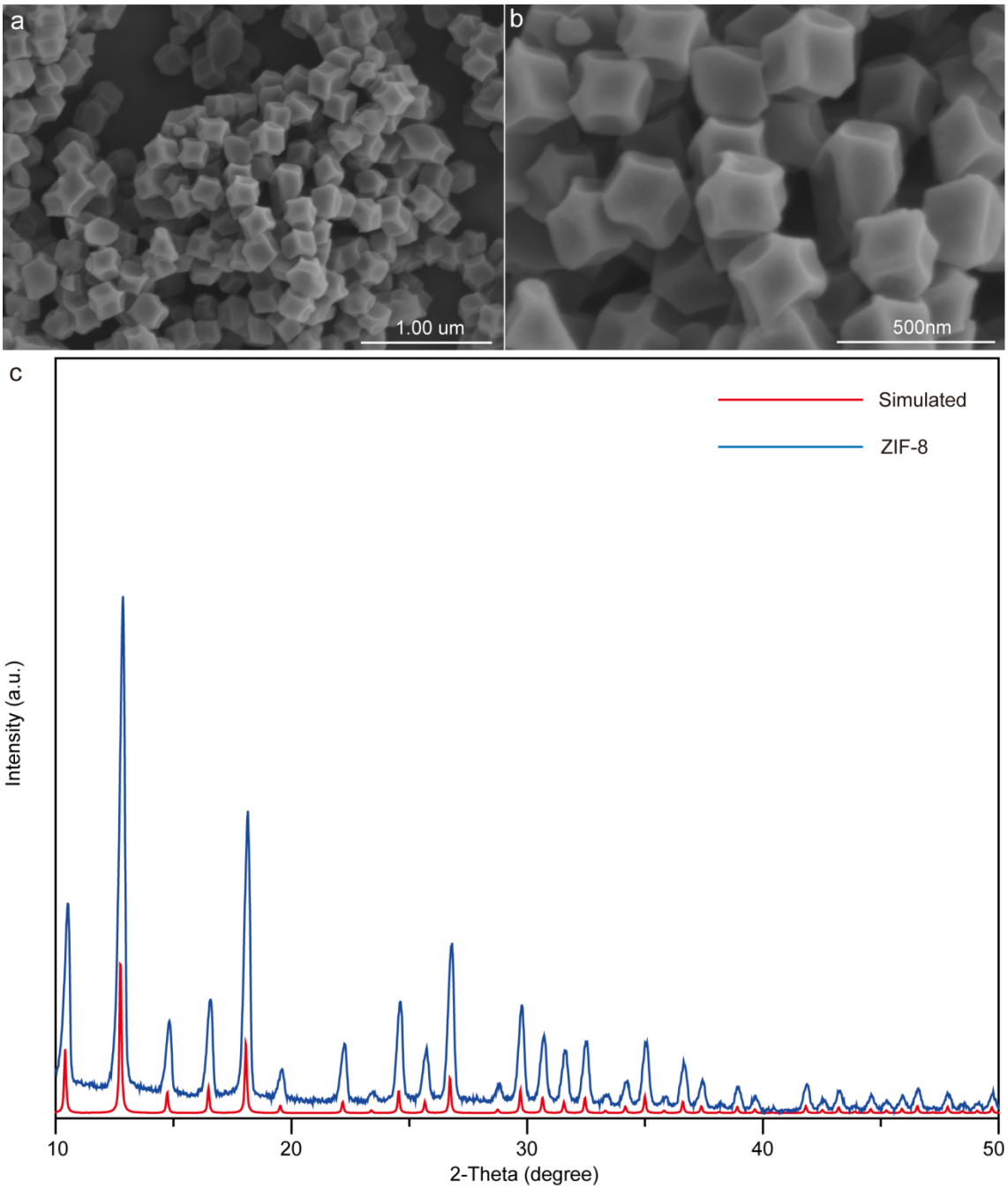

Figure S11. (a) SEM image and (b) high-magnification SEM image, (c) XRD pattern for the synthesized ZIF-8.

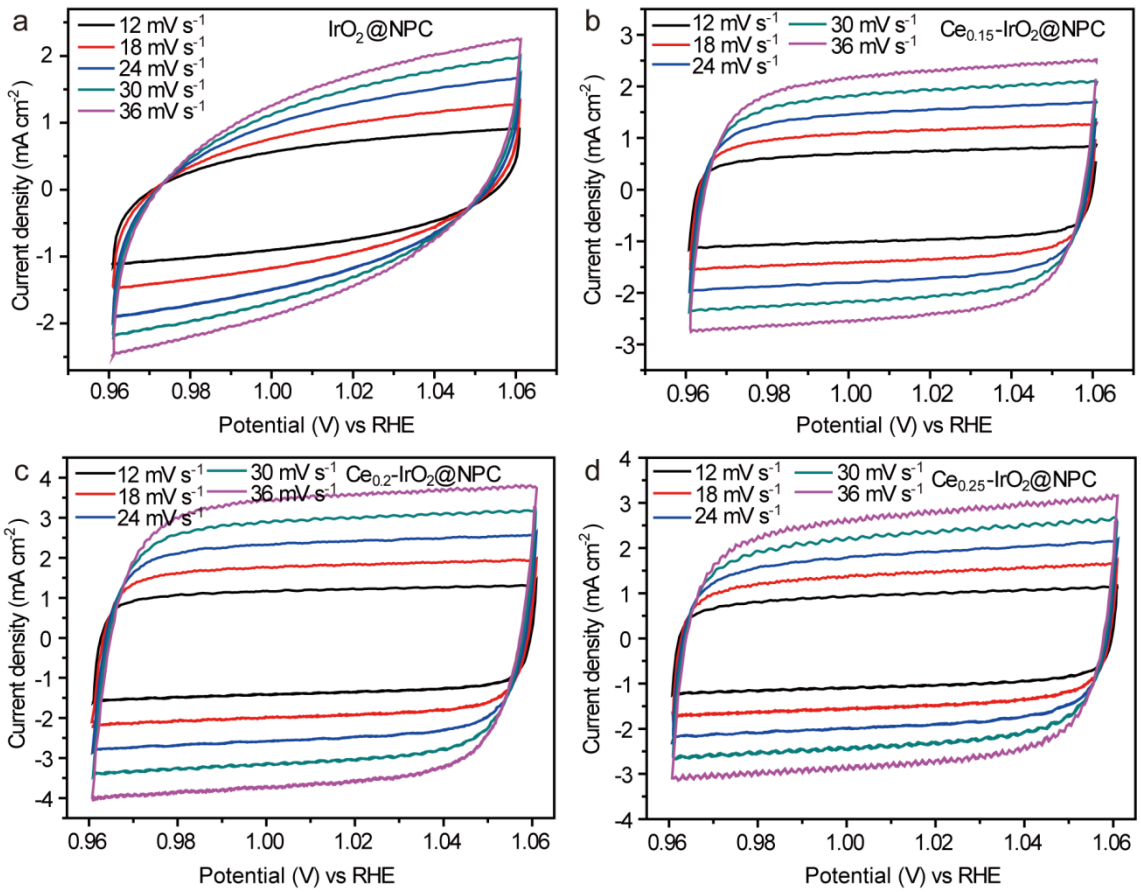

Figures S12. CV curves for (a) IrO_2@NPC, (b) $Ce_{0.15}$-IrO_2@NPC, (c) $Ce_{0.2}$-IrO_2@NPC, and (d) $Ce_{0.25}$-IrO_2@NPC from 12 mV s^{-1} to 36 mV s^{-1}.

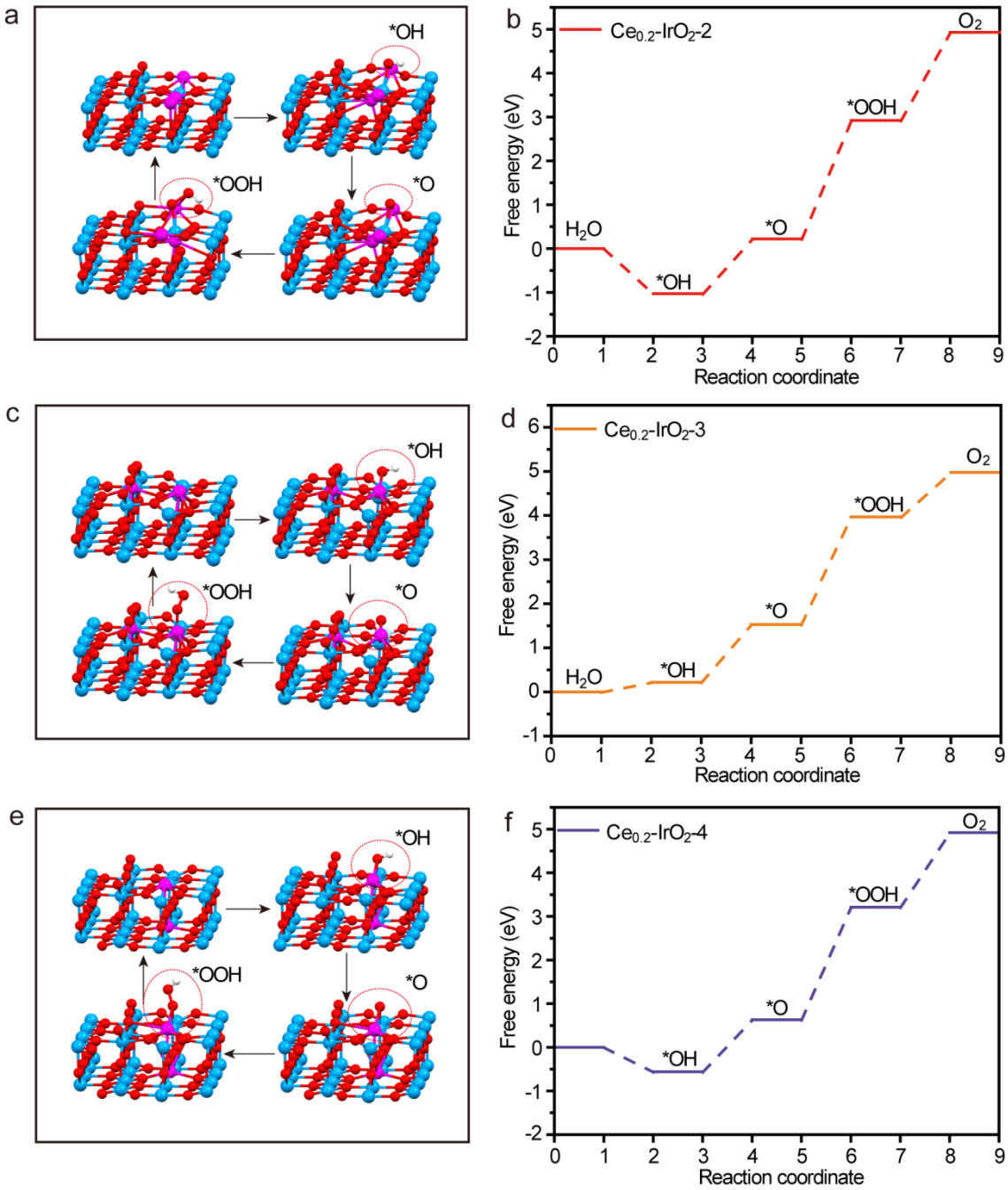

Figure S13. (a) The 4-step processes of OER for $Ce_{0.2}$-IrO_2-2, (b) The calculated Gibbs free-energy diagrams of $Ce_{0.2}$-IrO_2-2. (c) The 4-step processes of OER for $Ce_{0.2}$-IrO_2-3, (d) The calculated Gibbs free-energy diagrams of $Ce_{0.2}$-IrO_2-3. (e) The 4-step processes of OER for $Ce_{0.2}$-IrO_2-4, (f) The calculated Gibbs free-energy diagrams of $Ce_{0.2}$-IrO_2-4.

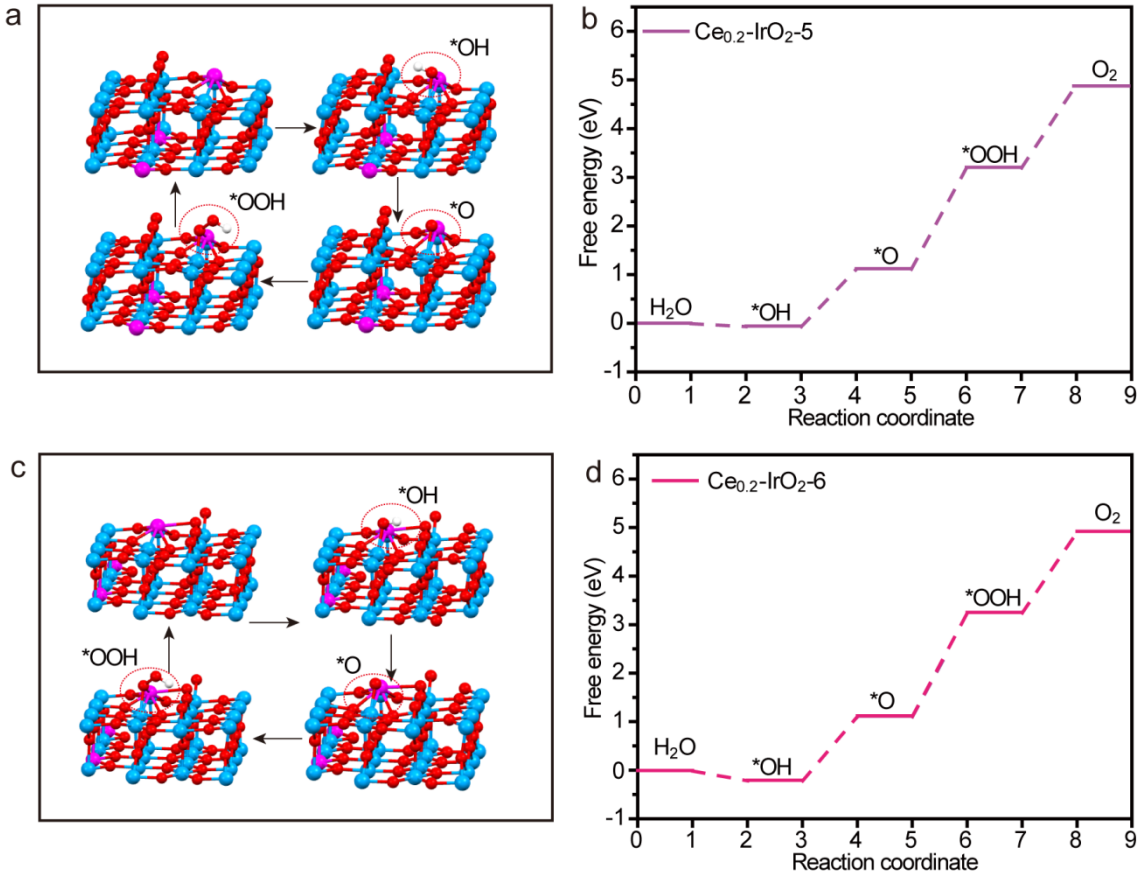

Figure S14. (a) The 4-step processes of OER for $Ce_{0.2}$-IrO_2-5, (b) The calculated Gibbs free-energy diagrams of $Ce_{0.2}$-IrO_2-5. (c) The 4-step processes of OER for $Ce_{0.2}$-IrO_2-6, (d) The calculated Gibbs free-energy diagrams of $Ce_{0.2}$-IrO_2-6.

Table S4. ICP analysis for the prepared $Ce_{0.2}$-IrO_2@NPC

Element	Sample amount	Conversion content	at.%
Ir	20 mg	15703.9	81.7
Ce	20 mg	2561.7	18.3

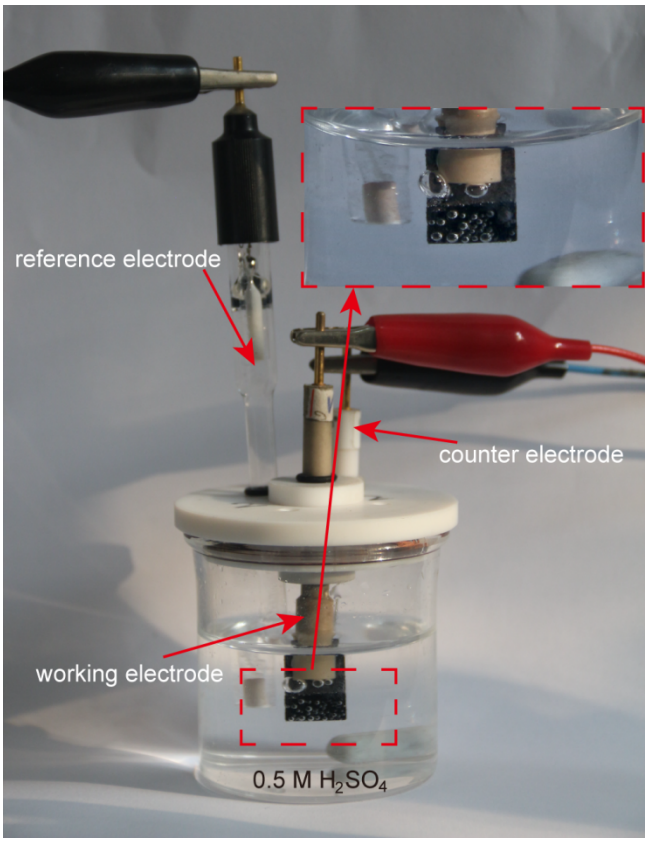

Figure S15. Three-electrode system for electrochemical measurements.

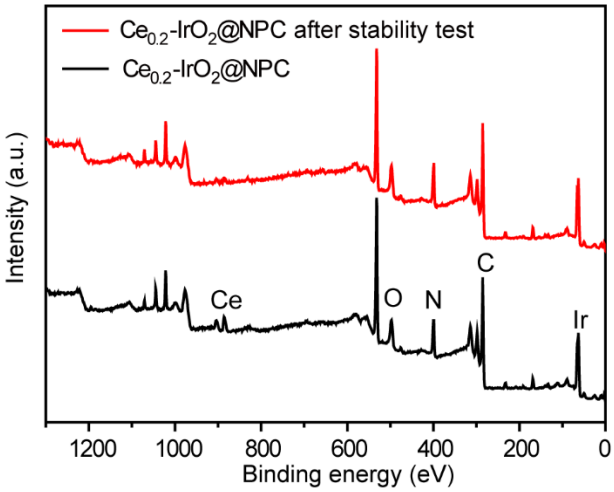

Figure S16. XPS spectra analysis for $Ce_{0.2}$-IrO_2@NPC and $Ce_{0.2}$-IrO_2@NPC after stability test.

The survey spectra in Figure S16 revealed the presence of C (52.27 at.%), O (29.44 at.%) for $Ce_{0.2}$-IrO_2@NPC, and the presence of C (52.29 at.%), O (30.59 at.%) for $Ce_{0.2}$-IrO_2@NPC after the stability test. The carbon to oxygen atomic ratios of $Ce_{0.2}$-IrO_2@NPC and $Ce_{0.2}$-IrO_2@NPC after stability test were calculated to be 1.77 and 1.71, respectively. The change of carbon to oxygen atomic ratio of $Ce_{0.2}$-IrO_2@NPC after stability indicates the carbon degradation during OER.

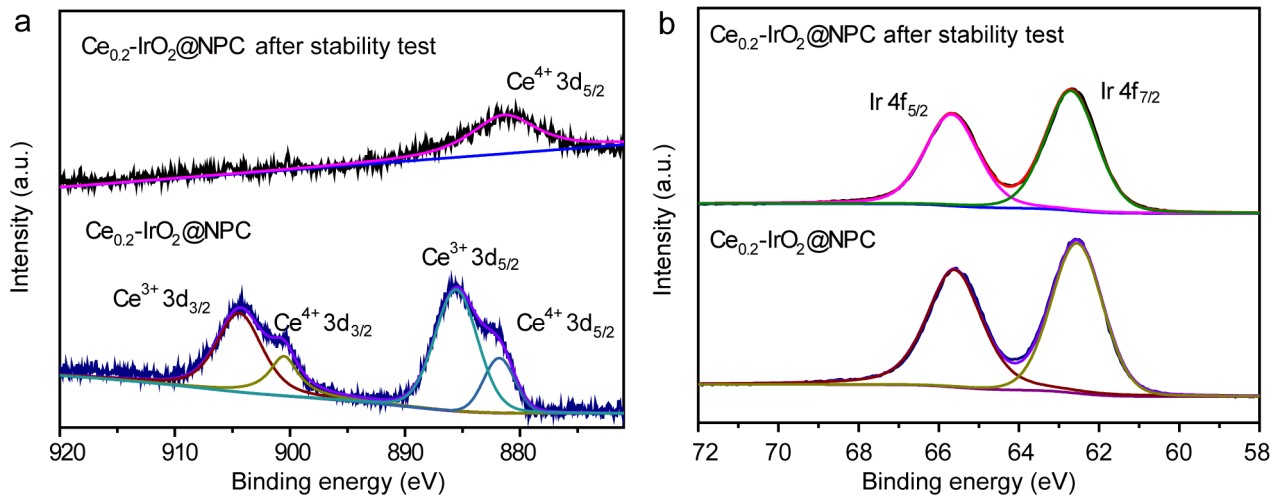

Figure S17. High-resolution XPS of (a) Ce 3d, (b) Ir 4f for $Ce_{0.2}$-IrO_2@NPC and $Ce_{0.2}$-IrO_2@NPC after stability test.

As shown in Figure S17, Ce in $Ce_{0.2}$-IrO_2@NPC all stayed Ce^{4+}, compared with Ce before OER test. This result revealed that Ce^{3+} in $Ce_{0.2}$-IrO_2@NPC before OER were all oxidized to Ce^{4+}. This can be attributed to the strong oxidation condition in acidic OER. Notably, the XPS of Ir 4f do not show obvious change after stability test, indicating the active site (Ir) kept its high stability.

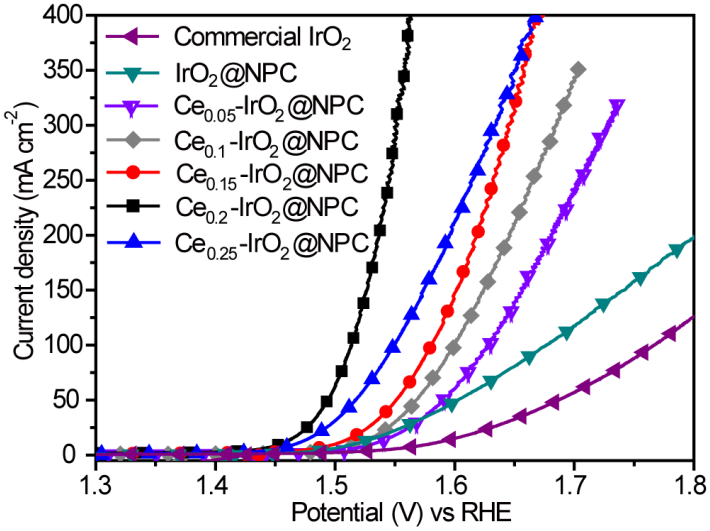

Figure S18 OER Polarization curves for these electrocatalysts in 0.5 M H_2SO_4.

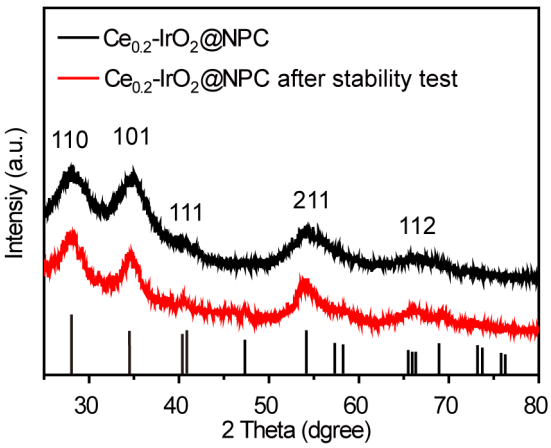

Figure S19 XRD patterns for $Ce_{0.2}$-IrO_2@NPC and $Ce_{0.2}$-IrO_2@NPC after stability test.

References

[1] X. Shi, H. Wang, P. Tang, B. Tang, Main reinforcement effects of precipitation phase Mg_2Cu_3Si, Mg_2Si and $MgCu_2$ on Mg-Cu-Si alloys by ab initio investigation, *Phy. B* **2017**, *521*, 339.

[2] G. Kresse, D. Joubert, From ultrasoft pseudopotentials to the projector augmented-wave method, *Phys. Rev. B* **1999**, *59*, 1758.

[3] J. Perdew, K. Burke, M. Ernzerhof, Generalized Gradient Approximation Made Simple, *Phy. Rev. Lett*. **1996**, *77*, 3865.

[4] D. Chadi, Special points for Brillouin-zone integrations, *Phys. Rev. B* **1977**, *16*, 5188.